Supporting Information

NiMOF integrated with conductive materials for efficient bifunctional electrocatalysis of urea oxidation and oxygen evolution reactions

Xiaopei Xie[1], Liqiang Xu[1,2], Qingsheng Zeng[1], Zhaona Zhang[1], Zhiqi Xu[1], Chuanxia Yin[3], Xinxing Wang*[,1,4]

1 Key Laboratory of Optic-electric Sensing and Analytical Chemistry for Life Science, MOE, Shandong Key Laboratory of Biochemical Analysis, College of Chemistry and Molecular Engineering, Qingdao University of Science and Technology, Qingdao 266042, China.

2 Shandong Tianyi Chemical Co., Ltd, Weifang 262737, China.

3 Marine Development and Fisheries Bureau of Kenli Distinct, Dongying 257500, China.

4 Xinjiang Blue Ridge Tunhe Degradable Materials Co., Ltd, Changji 831100, China.

* Corresponding auther

E-mail: wangxx@qust.edu.cn

1. Material characterization

SEM pictures was observed by a field emission scanning electron microscope (JSM-7610). XRD patterns were measured using a X-ray powder diffractometer (Rigaku D-MAX 2500/PC). XPS were recorded from a X-ray photoelectron spectrometer (Thermo ESCALAB 250XI) equipped with a standard monochromatic Al-Kα source (hv =1486.6 eV).

2. Product analysis

Chronoamperometry experiments were performed at 1.38 V vs. RHE for product analysis and faradaic efficiency (FE) determination. Electrolysis was carried out in a H-type electrolytic cell with an anionic membrane (Alkymer W-25) under Ar controlled atmosphere. MWCNT-NiMOF(Fc)/NF with a mass loading of 2 mg cm^{-2} was used as the working electrode. Hg/HgO electrode and platinum plate were employed as reference electrode and counter electrode, respectively. The anolyte and catholyte used were 1.0 mol L^{-1} KOH containing 0.33 mol L^{-1} urea, and the volume of solution in each compartment was 30 mL. Gas chromatography (GC 7900, Techcomp, Ar as carrier gas) was selected to analysis the produced N_2. NO_2^- were analyzed by ion chromatography (ICS-600, Thermo Scientific) with a Dionex IonPac AS19 – 4 μm 2 × 250 mm column and using 25 mmol L^{-1} KOH as the mobile phase.

The faradaic efficiency (FE) of reaction products was calculated from:

$$FE = \frac{m \times n \times F}{Q_{total}} \times 100\%$$

where n is the number of electrons transferred (6 for N_2 and NO_2^-), F Faraday constant, Q_{total} charge, and m total of product (mole).

3. Electrochemical measurements

All electrochemical tests were performed by a CHI 660E electrochemical workstation (Shanghai Chenhua) at room temperature. In a three-electrode system, a glassy carbon electrode (GCE) loaded with active material was used as working electrode, with a platinum sheet (1 cm × 1 cm) electrode as counter electrode and a Hg/HgO electrode as reference electrode. The measured potentials were converted to reversible hydrogen electrode (RHE) potentials by the following equation: $E_{RHE} = E_{Hg/HgO} + 0.098 + 0.059 \times pH$. The overall urea and water splitting electrolysis cell used a two-electrode system with Pt/C/NF as the cathode and MWCNT-NiMOF(Fc)/NF as the anode.

The working electrode was activated in electrolyte solution for 30 cycles at a scan rate of 100 mV s^{-1} between 1.06 V and 1.86 V. Linear sweep voltammetry (LSV) curves were obtained in electrolyte solution at a scan rate of 20 mV s^{-1}. Electrochemical impedance spectroscopy (EIS) measurements were conducted in 1.0 mol L^{-1} KOH solution, 1.0 mol L^{-1} KOH solution with 0.33 mol L^{-1} urea and different concentrations of KOH solution with 0.33 mol L^{-1} urea, respectively. In the three types of solutions mentioned above, the initial potentials for EIS testing were 1.50 V, 1.38 V and 1.38 V, respectively, with a frequency range from 100 KHz to 0.1 Hz and an amplitude of 5 mV. The long-term stability tests were measured using the chrono-potentiometric method. Double layer capacitance (C_{dl}) was calculated based on the cyclic voltammetry (CV) curves obtained in the apparently non-Faraday region at scan rates of 10, 20, 30, 40, and 50 mV s^{-1}. The current densities corresponding to

0.91 V were used for the calculation. Tafel plots of UOR and OER were extracted by LSV with a scan rate 5 mV s^{-1}. For OER, the backward sweep of the LSV scan was used for constructing the Tafel plot.

4. Equivalent circuit fitting results of Nquist plots obtained in urea solution

Table S1. Equivalent circuit fitting results of Nquist plots obtained in 1.0 mol L^{-1} KOH solution with 0.33 mol L^{-1} urea.

Electrodes	R_s (Ω cm^2)	R_1 (Ω cm^2)	R_2 (Ω cm^2)
MWCNT-NiMOF(Fc)	0.813	0.511	1.183
MWCNT-NiMOF	1.015	0.542	1.373
MWCNT/NiMOF(Fc)	1.154	1.722	2.283
NiMOF(Fc)	1.675	3.593	3.452
NiMOF	1.879	4.944	9.243

5. CV curves of the NiMOF-based material modified electrodes scanned in the non-Faraday interval

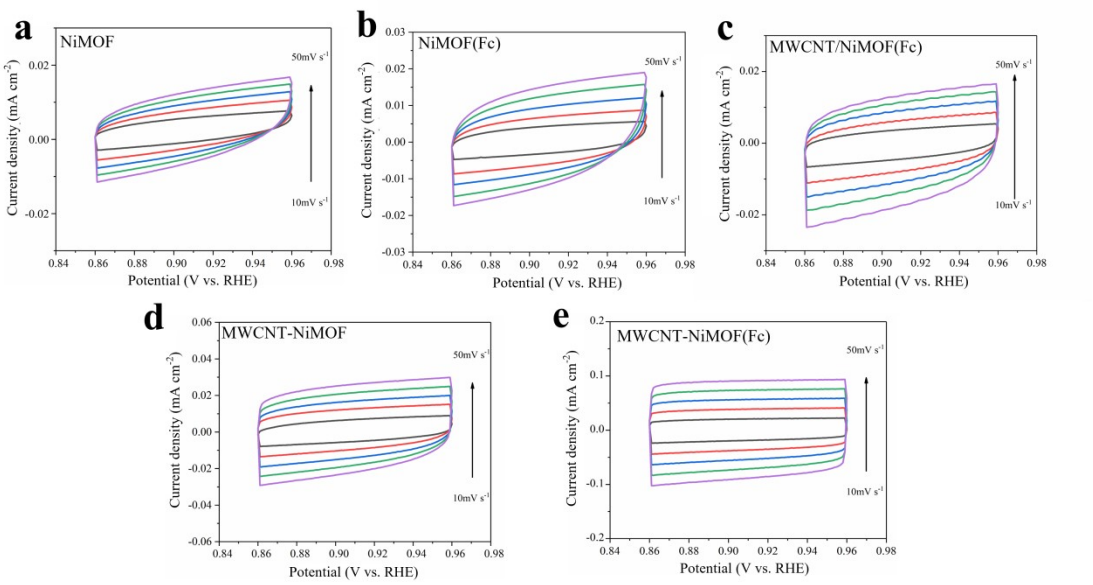

Figure S1. CV curves of (a) NiMOF/GCE, (b) NiMOF(Fc)/GCE, (c) MWCNT/NiMOF(Fc)/GCE (d) MWCNT-NiMOF/GCE, and (e) MWCNT-NiMOF(Fc)/GCE in 1.0 mol L^{-1} KOH with 0.33 mol L^{-1} urea at different scan rates.

6. Comparison of UOR catalytic activity of Ni-based electrocatalysts on GCEs

Table S2. Comparison of UOR catalytic activity of Ni-based electrocatalysts on GCEs.

Catalysts	Potential @ 10 mA cm^{-2} (V vs. RHE)	Current density @ 1.6 V (vs. RHE) (mA cm^{-2})	Electrolytes	Ref.
Ni-MOF	1.36	120	urea (0.33 mol L^{-1})	1
NiCr/C	1.38	90	urea (0.33 mol L^{-1})	2
β-$NiMoO_4$	1.498	-	urea (0.5 mol L^{-1})	3
Ni_2P	1.52	-	urea (0.33 mol L^{-1})	4
Ni/C-1	~1.35	95.47	urea (0.33 mol L^{-1})	5
Ni_2P	1.39	-	urea (0.33 mol L^{-1})	6
NiMn/C	1.40	42	urea (0.33 mol L^{-1})	7
Ni/Sn dendrites	1.41	-	urea (0.33 mol L^{-1})	8
porous rod-like Ni_2P/Ni	1.47	-	urea (0.33 mol L^{-1})	9
MWCNT-NiMOF(Fc)	1.38	173	urea (0.33 mol L^{-1})	This work

7. Forward sweep curve of LSV

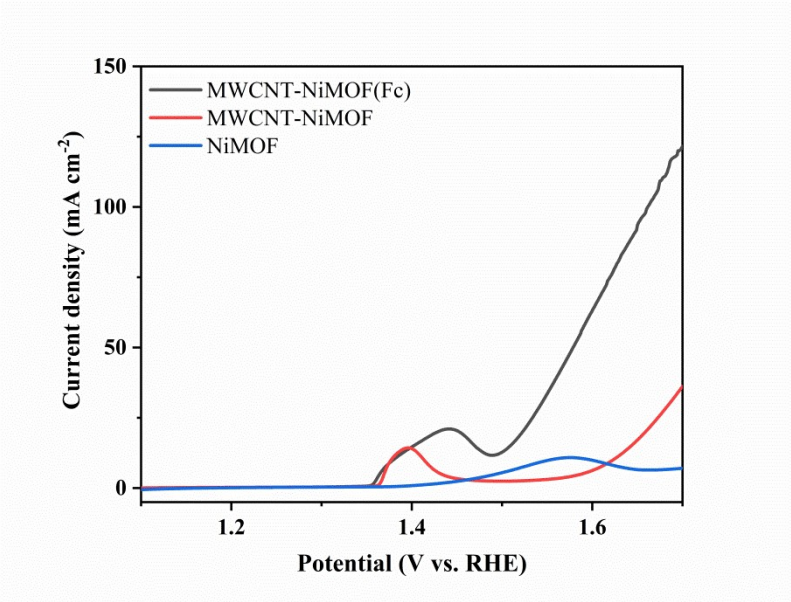

Figure S2. Forward scanning LSV curves of NiMOF/GCE, MWCNT-NiMOF/GCE, and MWCNT-NiMOF(Fc)/GCE in 1.0 mol L^{-1} KOH solution.

8. Equivalent circuit fitting results of Nquist plots obtained in KOH solution

Table S3. Equivalent circuit fitting results of Nquist plots obtained in 1.0 mol L^{-1} KOH solution.

Electrodes	R_s (Ω cm^2)	R_1 (Ω cm^2)	R_2 (Ω cm^2)
MWCNT-NiMOF(Fc)	0.991	0.618	0.778
MWCNT-NiMOF	1.218	0.783	3.671
NiMOF	2.010	2.881	10.563

9. Comparison of OER catalytic activity of Ni-based electrocatalysts on GCEs

Table S4. Comparison of OER catalytic activity of Ni-based electrocatalysts on GCEs.

Catalysts	Overpotential @ 10 mA cm^{-2} (mV)	Tafel slope (mV dec^{-1})	Electrolytes	Ref.
$Ni_{0.6}Co_{1.4}P$	300	80	KOH (1.0 mol L^{-1})	10
Ni-MOF(BTC)	346	64	KOH (1.0 mol L^{-1})	11
NP/NiO	332	65.6	KOH (1.0 mol L^{-1})	12
NiFe-LDH	275	56.7	KOH (1.0 mol L^{-1})	13
$Ni/CoMoS_4/Ni_3S_2$	338	53	KOH (1.0 mol L^{-1})	14
Ni-Doped AlOOH	320	63	KOH (1.0 mol L^{-1})	15
Ni-BDC@NiS	295	62	KOH (1.0 mol L^{-1})	16
Mo-Ni-Se	397	-	KOH (1.0 mol L^{-1})	17
$Co_{0.95}Cr_{0.05}Fe_2O_4$	293.3	76	KOH (1.0 mol L^{-1})	18
MWCNT-NiMOF(Fc)	274	42	KOH (1.0 mol L^{-1})	This work

10. Equivalent circuit fitting results of Nquist plots obtained in different concentrations of KOH solution with 0.33 mol L^{-1} urea

Table S5. Equivalent circuit fitting results of Nquist plots obtained in different concentrations of KOH solution with 0.33 mol L^{-1} urea.

Concentrations of KOH (mol L^{-1})	Rs (Ω cm^2)	R_1 (Ω cm^2)	R_2 (Ω cm^2)
0.25	0.889	3.877	2.374
0.5	0.478	1.351	1.784
1.0	0.276	0.703	0.776
2.0	0.178	0.583	0.856
3.0	0.121	0.643	0.667
4.0	0.096	0.598	0.784
5.0	0.108	1.196	0.799

11. Calibration curves for N_2 and NO_2^- determination

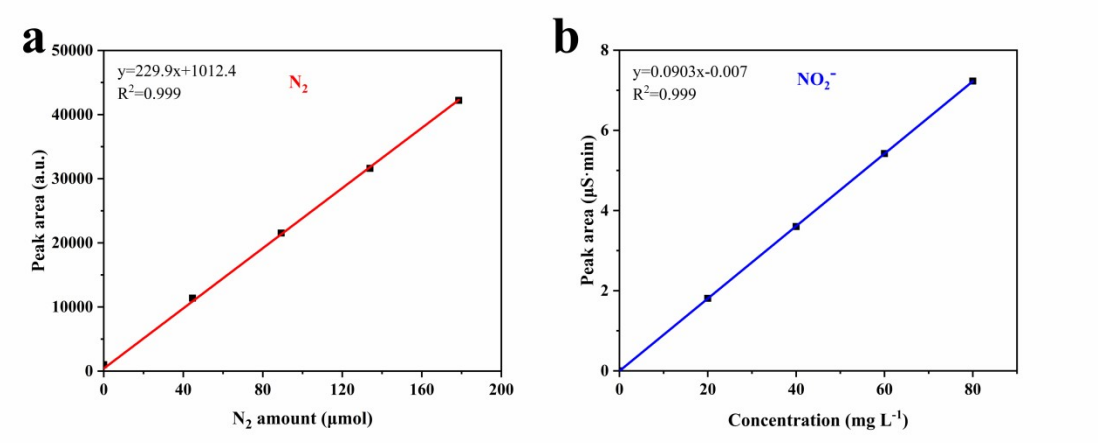

Figure S3. Calibration curves for N_2 (a) and NO_2^- (b) determination.

12. Faradaic efficiency of N_2 and NO_2^-

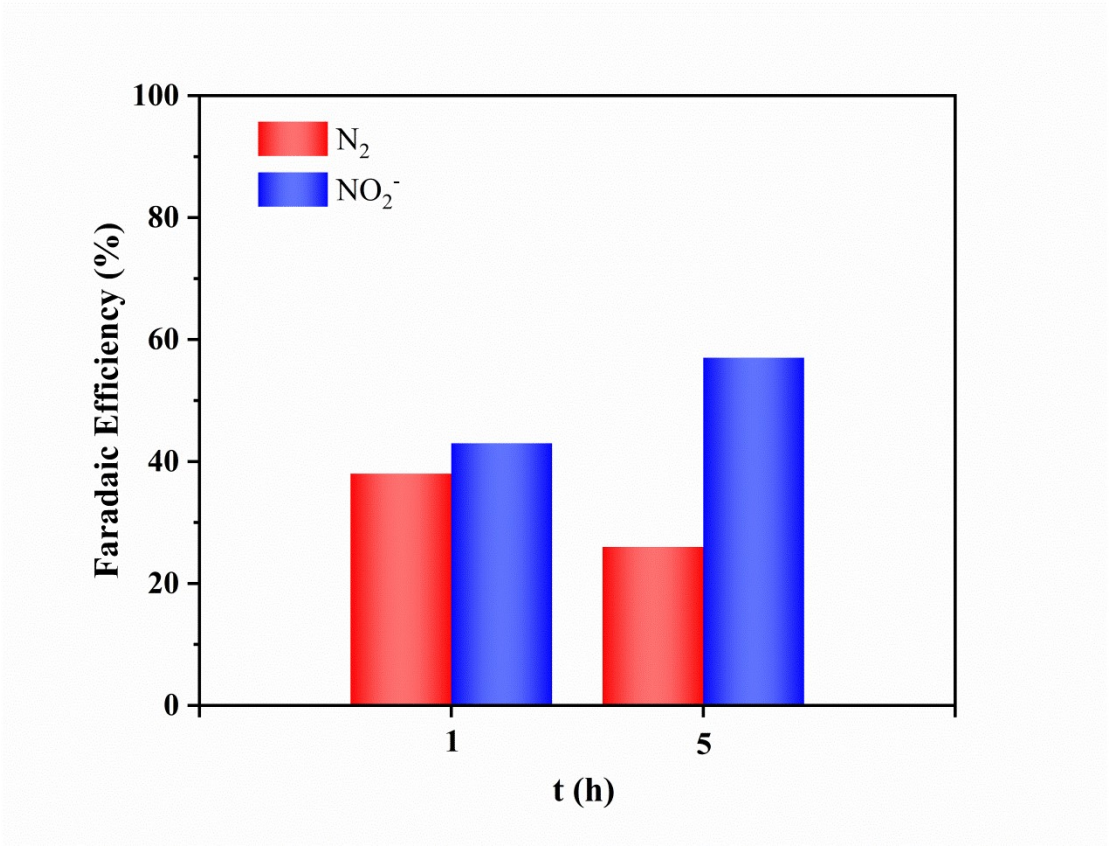

Figure S4. Faradaic efficiency of N_2 and NO_2^-

References

1. D. Zhu, C. Guo, J. Liu, L. Wang, Y. Du and S. Z. Qiao, *Chemical Communications*, 2017, **53**, 10906-10909.
2. R. K. Singh and A. Schechter, *ChemCatChem*, 2017, **9**, 3374-3379.
3. K. Hu, S. Jeong, G. Elumalai, S. Kukunuri, J.-i. Fujita and Y. Ito, *ACS Applied Energy Materials*, 2020, **3**, 7535-7542.
4. H. Liu, S. Zhu, Z. Cui, Z. Li, S. Wu and Y. Liang, *Nanoscale*, 2021, **13**, 1759-1769.
5. L. Wang, L. Ren, X. Wang, X. Feng, J. Zhou and B. Wang, *ACS Applied Materials & Interfaces*, 2018, **10**, 4750-4756.
6. D. Yang, Y. Gu, X. Yu, Z. Lin, H. Xue and L. Feng, *ChemElectroChem*, 2018, **5**, 659-664.
7. N. A. M. Barakat, M. Alajami, Y. Al Haj, M. Obaid and S. Al-Meer, *Catalysis Communications*, 2017, **97**, 32-36.
8. R. K. Singh, P. Subramanian and A. Schechter, *ChemElectroChem*, 2017, **4**, 1037-1043.
9. Q. Li, X. Li, J. Gu, Y. Li, Z. Tian and H. Pang, *Nano Research*, 2020, **14**, 1405-1412.
10. B. Qiu, L. Cai, Y. Wang, Z. Lin, Y. Zuo, M. Wang and Y. Chai, *Advanced Functional Materials*, 2018, **28**, 1706008.
11. V. Maruthapandian, S. Kumaraguru, S. Mohan, V. Saraswathy and S. Muralidharan, *ChemElectroChem*, 2018, **5**, 2795-2807.
12. P. Bhanja, Y. Kim, B. Paul, Y. V. Kaneti, A. A. Alothman, A. Bhaumik and Y. Yamauchi, *Chemical Engineering Journal*, 2021, **405**, 126803.
13. M. Liu, L. Kong, X. Wang, J. He and X. H. Bu, *Small*, 2019, **15**, 136336.
14. P. Hu, Z. Jia, H. Che, W. Zhou, N. Liu, F. Li and J. Wang, *Journal of Power Sources*, 2019, **416**, 95-103.
15. Y. Zhou and H. C. Zeng, *ACS Sustainable Chemistry & Engineering*, 2019, **7**, 5953-5962.
16. P. He, Y. Xie, Y. Dou, J. Zhou, A. Zhou, X. Wei and J. R. Li, *ACS Applied Materials & Interfaces*, 2019, **11**, 41595-41601.
17. H. Yang, Y. Huang, W. Y. Teoh, L. Jiang, W. Chen, L. Zhang and J. Yan, *Electrochimica Acta*, 2020, **349**, 136336.
18. S. Pan, J. Yu, Y. Zhang and B. Li, *Materials Letters*, 2020, **262**, 127027.